Continuous Aircraft Positioning Using GPS Aided by INS

Final Report

State Job # 14643(0), Contract No. 8403
OSU Research Foundation Project 732280

Submitted to

Ohio Department of Transportation
Office of Research and Development
25 South Front Street, P.O. Box 899
Columbus, Ohio 43216-0899

by

Christopher Jekeli, Associate Professor
Department of Civil and Environmental Engineering
and Geodetic Science
The Ohio State University
2070 Neil Avenue
Columbus, Ohio 43210-1275

tel: 614-292-6753, fax: 614-292-2957

23 January 1998

1. Report No.		3. Recipient's Catalog No.
FHWA/OH-98/008	PB99-106726	
4. Title and Subtitle CONTINUOUS AIRCRAFT POSITIONING USING GPS AIDED BY INS		5. Report Date January 23, 1998
		6. Performing Organization Code
7. Author(s) Christopher Jekeli		8. Performing Organization Report No. 10. Work Unit No. (TRAIS)
9. Performing Organization Name and Address The Ohio State University Department of Geodetic Science and Surveying Columbus, OH 43210-1247		11. Contract or Grant No. State Job No. 14643(0) 13. Type of Report and Period Covered Final Report
12. Sponsoring Agency Name and Address Ohio Department of Transportation 25 S. Front St. Columbus, OH 43215		14. Sponsoring Agency Code

15. Supplementary Notes

Prepared in cooperation with the U.S. Department of Transportation, Federal Highway Administration

16. Abstract

This report presents the results of a study performed at the Department of Civil and Environmental Engineering and Geodetic Science with application to ODOT's Aerial Engineering tasks. Specifically, the study was concerned with the integration of the Global Positioning System and an inertial navigation system (INS) for precise, continuous positioning of ODOT's aerial photogrammetric airplane. The study was based on testing a medium-to-high accuracy inertial navigation system (Litton's LN93) with GPS on board an aircraft. The objective was to demonstrate that such an integration can maintain the GPS accuracy of 2-3 cm over short intervals (few seconds) and to determine the capability using optimal estimation algorithms of maintaining accurate positions over somewhat longer periods. The motivation behind this study is the fact that GPS positioning may be interrupted because of a variety of reasons, from electronic interference (causing cycle slips) to shadowing of the satellite signals (by aircraft wings and tail).

The results of the study, which are based on actual test flights with a similar system, the LN100, indicate clearly that such continuous positioning is possible with a loosely integrated GPS/INS configuration. However, it is also noted that the integration cannot be completely uncoupled and requires a comprehensive filtering and smoothing algorithm in order to estimate the INS errors. Other results include recommendations on the quality of the INS needed for such application and the opportunity to extract orientation information from the estimation algorithm.

17. Key Words	18. Distribution Statement
Global Positioning System, Inertial Navigation System, continuous positioning, photogrammetry, Kalman filter, Kalman smoother	No Restrictions. This document is available to the public through the National Technical Information Service, Springfield, Virginia 22161

19. Security Classif. (of this report)	20. Security Classif. (of this page)	21. No. of Pages	22. Price
Unclassified	Unclassified		

Continuous Aircraft Positioning Using GPS Aided by INS

ODOT State Job # 14643(0)

Christopher Jekeli
Department of Civil and Environmental Engineering
and Geodetic Science
The Ohio State University
2070 Neil Avenue
Columbus, Ohio 43210-1275

tel: 614-292-6753, fax: 614-292-2957

23 January 1998

Executive Summary

This report presents the results of a study performed at the Department of Civil and Environmental Engineering and Geodetic Science with application to ODOT's Aerial Engineering tasks. Specifically, the study was concerned with the integration of the Global Positioning System (GPS) and an inertial navigation system (INS) for precise, continuous positioning of ODOT's aerial photogrammetric airplane. The study was based on testing a medium-to-high accuracy inertial navigation system (Litton's LN93) with GPS on board an aircraft. The objective was to demonstrate that such an integration can maintain the GPS accuracy of 2-3 cm over short intervals (few seconds) and to determine the capability using optimal estimation algorithms of maintaining accurate positions over somewhat longer periods. The motivation behind this study is the fact that GPS positioning may be interrupted because of a variety of reasons, from electronic interference (causing cycle slips) to shadowing of the satellite signals (by aircraft wings and tail).

This report first reviews the essential measurement characteristics of both the GPS and the INS. This is followed by a mathematical treatment of the integration of data from both systems to achieve continuous positioning of the vehicle. The mathematical estimation methods are then applied to data collected from systems deployed on an aircraft in order to demonstrate the levels of position errors.

The results of these studies indicate clearly that such continuous positioning is possible with a loosely integrated GPS/INS configuration. However, it is also noted that the integration cannot be

completely uncoupled and requires a comprehensive filtering and smoothing algorithm in order to estimate the INS errors. In fact, in order to achieve the predicted GPS accuracy capability of 2 - 3 cm on a continuous basis requires a high-order optimal estimation algorithm that correctly models the drift and bias errors of the INS. Accuracies of 10 cm, or better, have been demonstrated for GPS outages up to 30 seconds. This is also entirely adequate to recover from cycle slips over that interval, since it represents only half of one wavelength of the carrier wave. Other results of the study include recommendations on the quality of the INS needed for such application and the opportunity to extract orientation information from the estimation algorithm.

The next step in this development is the construction of a fully dedicated system for operational implementation, similar to the one tested, including an operational software package that can be used routinely to process the GPS and INS data in an optimal and flexible manner.

PREFACE

This report presents the results of a study performed at the Department of Civil and Environmental Engineering and Geodetic Science with application to ODOT's Aerial Engineering tasks. Specifically, the study was concerned with the integration of the Global Positioning System and an inertial navigation system (INS) for precise, continuous positioning of ODOT's aerial photogrammetric airplane. The study was based on testing a medium-to-high accuracy inertial navigation system (Litton's LN93) with GPS on board an aircraft. The objective was to demonstrate that such an integration can maintain the GPS accuracy of 2-3 cm over short intervals (few seconds) and to determine the capability using optimal estimation algorithms of maintaining accurate positions over somewhat longer periods. The motivation behind this study is the fact that GPS positioning may be interrupted because of a variety of reasons, from electronic interference (causing cycle slips) to shadowing of the satellite signals (by aircraft wings and tail).

The results of the study, which are based on actual test flights with a similar system, the LN100, indicate clearly that such continuous positioning is possible with a loosely integrated GPS/INS configuration. However, it is also noted that the integration cannot be completely uncoupled and requires a comprehensive filtering and smoothing algorithm in order to estimate the INS errors. Other results include recommendations on the quality of the INS needed for such application and the opportunity to extract orientation information from the estimation algorithm.

The next step in this development is the construction of a fully dedicated system for operational implementation, similar to the one tested.

Christopher Jekeli

Table of Contents

Table of Contents (continued)

List of Tables

List of Figures

CHAPTER 1

INTRODUCTION

The Ohio Department of Transportation (ODOT), Aerial Engineering Facility, has a requirement to position a photogrammetrically equipped aircraft to an accuracy of 2 cm (1 sigma) in all three coordinates relative to given base station coordinates at specific epochs defined by the opening of the camera shutter.

Tests using Global Positioning System (GPS) methods have demonstrated this positioning accuracy under suitable conditions. It is achievable because the positions are based on the continuously tracked phase of the 19-cm carrier wave of the GPS transmissions. Conditions that would encumber achieving this accuracy with GPS include unavoidable electronic interferences that cause cycle slips, or full-cycle discontinuities, in the tracked phase, which results in the loss of the integer count of full cycles. This so-called full-cycle ambiguity (needing resolution, in any case, at the initial epoch) usually can again be resolved with special data processing methods, e.g., using the coded signal and the signal transmitted at the second frequency. However, this renewal requires several epochs (tens of seconds and longer) of data, depending on the GPS receiver and satellite configuration. Once reacquired, the full-cycle count is usable backwards (post-mission, only) to the epoch of the cycle slip. Another condition inhospitable to maintaining accurate GPS positioning is loss of signal due to temporary shadowing (e.g., by aircraft wings), thus possibly reducing the number of tracked satellites to fewer than required for positioning (this is not a usual occurrence, more so for ground vehicles passing larger obstructions).

The relatively long time interval between GPS-derived positions (1 second or longer) implies a significant asynchronism with respect to the epochs of the opening of the camera shutter. The magnitude of this problem becomes apparent considering that a mere 0.02 g acceleration of the aircraft causes a 2.5 cm variation in position in a span of only 0.5 sec. Thus, even a 1-sec. integration time poses interpolation problems. Also to consider is that an aircraft flying at 225 mi/hr traverses 100 m between GPS position fixes spaced 1 second apart.

In summary, the required accuracy based on GPS positioning alone is compromised in at least two important ways: 1) cycle slips that span intervals too short to enable full-cycle ambiguity resolution may cause the GPS solution to be severely inaccurate or even non-existent within that interval (depending on the number of satellites available); and 2) the integration time of 1 second or longer may be too long to permit accurate interpolation of position to the epoch of interest (e.g., the time of camera shutter opening).

It is widely recognized that the integration of GPS with an inertial navigation system (INS) can alleviate these shortcomings in positioning. Positions and velocities from an INS are obtained by integrating accelerations sensed by accelerometers. Typically, these systems yield output rates on the order of 100 Hz (or more), are very precise in the short term, and, therefore, serve as excellent position interpolators. Moreover, the operation of an INS is completely autonomous, meaning that the position solution is obtained entirely from the unit, in principle, without additional external information. Only initial position and velocity must be known. Finally, the INS provides angular data from a set of gyroscopes whose primary intent is to orient the accelerometers, but can also be used to orient the GPS antenna with respect to local level. The major drawback of INS positioning

is accuracy degradation with time, where the amount of degradation for a system ultimately is a function of sensor quality, and hence, sensor cost. However, the positioning requirements stated above are for short periods, on the order of several seconds to minutes, where even a low-to-medium accuracy INS could be effective.

The integration of GPS and INS is fast becoming the mode of operation for aerial photogrammetric surveys (see Jekeli, 1995, for a broad overview). Primarily, INS is used to recover quickly from cycle slips in the GPS data. In fact, the integration of GPS and INS has long been recognized as providing robustness and added value to any platform requiring accurate and uninterrupted positions, velocities, and orientation. The demonstrations of such integrations have been reported consistently at national and international symposia and conferences in navigation and positioning. As a relevant sample, it is worth mentioning the results of Schwarz et al. (1994), who demonstrate the capability of INS data processing for cycle slip recovery. Their tests were done using a ground vehicle and they show that position accuracy better than 10 cm during GPS outages up to two minutes were maintained with the INS and a backward smoothing algorithm. Another study was performed by Söhne and Heinze (1995) who also demonstrate INS bridging capability during GPS outages using a ground vehicle. With only a filter algorithm (not smoothing), they show that INS can maintain up to 60 cm position accuracy within one minute of GPS outage. Both of these results (done with ground vehicles) were based on a similar INS as used for this study.

The intent here is to demonstrate the integration of INS and GPS for ODOT's airborne accuracy requirements where the INS is used as an interpolator between GPS epochs as well as an extrapolator / interpolator during GPS outages, thus better defining the aircraft position at the time of camera shutter opening, and providing accurate capability to recover from cycle slips and other lapses in GPS positioning. This project was motivated in part by the availability of a medium-to-high accuracy INS. One system, model LN93, is on loan from Litton Guidance and Control; and a second Litton system, model LN100, was obtained by OSU's Center for Mapping to develop an Airborne Integrated Mapping System (AIMS). Both of these systems were used to analyze the integration of GPS and INS and determine the positioning capabilities of this integration.

The studies were limited to the loosely integrated concept with the goal of yielding an uninterrupted aircraft positioning capability (post-mission) at the accuracy of 2-3 cm over short (on the order of a few seconds) intervals. This accuracy is commensurate with the accuracy available from precision GPS alone under normal operating conditions, and the intent is to demonstrate the transfer of positioning accuracy from the GPS epochs to any intermediate epoch (the time of shutter opening) and to bridge other positioning gaps in the GPS data stream. In addition, the test results will identify the important characteristics of the INS needed for this type of application, as well as other survey applications, e.g., positioning ground vehicles subjected to longer GPS outages.

This final report reviews the essential instrumentation components, both GPS and INS, including the data output and their integration for accurate continuous positioning. The results of the studies show the benefit of using INS to interpolate between GPS position determinations and are based on actual flight tests conducted by the Center for Mapping. These results then lead to specification for an INS suitable for improving the positioning of an operational aerial photogrammetric platform. In addition, software algorithms needed to perform the integration of the GPS/INS data are described and form the basis for future design and implementation. These specifications and software algorithms can be implemented to design an optimal cost-effective mechanization of an operational integrated GPS/INS for the airborne platform.

CHAPTER 2

THE GLOBAL POSITIONING SYSTEM

2.1 Introduction

The Global Positioning System (GPS) comprises a set of orbiting satellites which may be thought of as active beacons in space transmitting signals that when observed on the Earth (or anywhere in space where the satellites are in view) provide information about the distance between the satellite and the observer. With favorable geometry among the satellites and the observer and with error-free and time-synchronized instrumentation, three distances to distinct satellites whose positions are known enable a solution of the observer's position by the method of intersection. This concept is basic to the now standard practice of geodetic static surveying and has been demonstrated to yield precise positioning of aircraft and other vehicles that carry scientific as well as surveying (photogrammetric and remote sensing) types of instrumentation (e.g., Yang, 1995).

2.2 Kinematic Positioning

Kinematic positioning refers to GPS positioning of a moving vehicle or platform. One could attempt this either in real time, that is, instantaneously, or usually with higher accuracy in a post-mission mode. The term *navigation* is used to refer to the real-time processing of the positioning data, while kinematic *positioning* is reserved for the post-processing of the data (as computers become more powerful, the distinction may become rather nebulous).

The observables are the same whether in static or kinematic positioning. The differences do include, however, the loss of the benefit of time averaging that yields higher accuracy per point in the static case and the need to increase the bandwidth of the tracking loop to accommodate the high frequency dynamics of the vehicle. (On the other hand, we are not interested in high-dynamic vehicles, such as military fighter aircraft.) In addition, kinematic GPS positioning often is burdened by a more restrictive and changing environment in terms of visible satellites, interference from passing structures, and multipath. This, of course, is one of the reasons for integration with INS.

2.3 The GPS Observables and Unknowns

The GPS receiver measures the correlation between the received satellite signal codes and identical codes that are generated by the receiver and synchronized to the codes generated in the satellite. The correlation is highest when the incoming codes are shifted in time to account for the time of their transit from the satellite to the receiver. The amount of this imposed time delay, obtained from the maximum code correlation, then represents the time of transit of the satellite codes from the satellite to the receiver; and when multiplied by the speed of light in vacuum yields the satellite-to-receiver distance. Because in reality there are errors such as clock errors, propagation medium effects, multipath, and receiver electronic delays, the measured delay represents not the true range, but the *pseudorange*, between receiver and satellite.

If t represents true time (GPS time), then let $\tau_r(t)$ be the time of reception of the signal as indicated by the clock of the r^{th} receiver, and let $\tau^p(t - \Delta t_r^p)$ be the time of transmission of that same signal as indicated on the clock of the p^{th} satellite. The time of transmission on this clock is supposed to be the true time minus the actual time of transit of the signal, Δt_r^p. Notationally, it is convenient as well as conventional to let superscripts identify quantities referring to satellites and to let subscripts identify quantities referring to receivers. Quantities with both superscript and subscript depend on both satellite and receiver.

It can be shown (Leick, 1995) that the pseudorange, s_r^p, at the receiver-indicated time is given by

$$s_r^p(\tau_r) = \rho_r^p(\tau_r) + c\left(\Delta\tau_r - \Delta\tau^p\right) - \dot{\rho}_r^p \Delta\tau_r + \Delta\rho^p_{offset,r} + \Delta\rho^p_{iono,r} + \Delta\rho^p_{tropo,r} + \Delta\rho^p_{m.path,r} + \Delta\rho^p_{equip,r} + \varepsilon^p_{\rho,r} \tag{2.1}$$

where ρ_r^p is the true range at the indicated time, $\Delta\tau_r$ is the receiver clock error, $\Delta\tau^p$ is the satellite clock error, $\dot{\rho}_r^p \Delta\tau_r$ accounts for the fact that the true range is different at the indicated and true time epochs, $\Delta\rho^p_{offset,r}$ is an error due to antenna center offsets, $\Delta\rho^p_{iono,r}$ is the error due to ionospheric refraction, $\Delta\rho^p_{tropo,r}$ is the error due to tropospheric refraction, $\Delta\rho^p_{m.path,r}$ is the multipath effect, $\Delta\rho^p_{equip,r}$ represents signal delays within the equipment electronics, and $\varepsilon^p_{\rho,r}$ is the random noise of the measurement. Some of these errors can be calibrated or compensated fairly readily, using different frequencies or models. Others, in particular the multipath, are notoriously difficult to deal with.

A pseudorange observable, as shown in (2.1), is available for each of the transmitted codes, the C/A code, as well as the P-codes on the L1 and L2 carriers, on appropriately equipped receivers.

The GPS codes are transmitted on carrier signals whose phase can be measured with respect to nearly identical signals generated by the receiver. Thus, another type of observable available on all geodetic receivers is the difference between the phase of the receiver-generated carrier signal at the time of reception and the phase of the satellite signal at the time of transmission (which arrives at the receiver unaltered except for the propagation effects that similarly corrupt the code measurement). The difference in phases, again, is due to the time of transit of the signal. Actually, the phase tracking loop of the receiver, when it first locks on to the signal, has no way of knowing the integer number of full cycles that comprise the difference in phases. Therefore, the absolute range to the satellite cannot be determined directly on the basis of the phase measurement. On the other hand, once acquired, the signal is tracked continuously and the complete cycles are counted and added to the measurement of the fractional phase difference.

It can be shown (Leick, 1995) that the accumulated carrier phase observable, ϕ_r^p, is given by

$$\phi_r^p(\tau_r) = \frac{f_0}{c}\rho_r^p(\tau_r) + f_0\left(\Delta\tau_r - \Delta\tau^p\right) + \phi_{0,r} - \phi_0^p - N_r^p - \frac{f_0}{c}\dot{\rho}_r^p \Delta\tau_r + \Delta\phi^p_{offset,r} + \Delta\phi^p_{iono,r} + \Delta\phi^p_{tropo,r} + \Delta\phi^p_{m.path,r} + \Delta\phi^p_{equip,r} + \varepsilon^p_{\phi,r} \tag{2.2}$$

where f_0 is the nominal frequency, c is the speed of light, $\phi_{0,r}$ and ϕ_0^p are receiver and satellite

phase offsets, N_r^p is the integer also known as the *carrier phase ambiguity* representing the unknown full number of cycles at the *initial* time of phase lock, $\varepsilon_{\phi,r}^p$ is the phase measurement error, and the other errors are analogous to the corresponding pseudorange errors. A carrier phase observable such as given in (2.2) holds for both L1 and L2 carriers, where, of course, the nominal frequency, f_0, as well as the phase error terms are different in each case.

2.4 Combinations of Observations

Inspecting the measurement equations for the pseudorange and carrier phase, one sees some quantities that do not change, such as clock biases and the phase ambiguity, or that change more slowly or have a long correlation time, such as tropospheric delays. In addition, there are terms common to observations that correspond to different receiver-satellite combinations. One could use each observation of pseudorange or carrier phase and try to solve for (or model or ignore) unknown error terms to the extent possible using observations to different satellites. This is known as *absolute positioning*. Or, what turns out to be more accurate in a relative sense, one could take differences between observations thus canceling the common mode terms and greatly reduce the effects of slowly varying error terms. This is known as *relative positioning*. In kinematic positioning, this means that one receiver is stationary and one receiver, the *rover*, is moving. Relative kinematic positioning has its limitations for a given tolerance in accuracy. The larger the baseline between rover and stationary receiver, the less is the cancellation of certain correlated errors, such as tropospheric delays and satellite orbit error (that is, they become uncorrelated).

To investigate the relationships between certain unknowns and the observations, or combinations thereof, consider again the pseudorange (2.1) with some of the error terms excluded:

$$s_r^p(\tau_r) = \rho_r^p(\tau_r) + c\left(\Delta\tau_r(t) - \Delta\tau^p(t - \Delta t_r^p)\right) + \Delta\rho_{iono,r}^p + \varepsilon_{\rho,r}^p \tag{2.3}$$

Similarly, the phase observable (2.2) simplifies to

$$\phi_r^p(\tau_r) = \frac{f_0}{c}\rho_r^p(\tau_r) + f_0\left(\Delta\tau_r(t) - \Delta\tau^p(t - \Delta t_r^p)\right) + \phi_{0,r} - \phi_0^p - N_r^p + \Delta\phi_{iono,r}^p + \varepsilon_{\phi,r}^p \tag{2.4}$$

Each observable, whether code or phase, is a function of the range between the receiver and the satellite, but also of the additional parameters, including the clock errors, the phase offsets, the initial phase ambiguity, and the ionospheric delay. These so-called nuisance parameters can be solved only if at least as much information (independent observations) is available as unknown parameters.

Additional information comes in many forms. By observing additional ranges to other satellites, the receiver clock error can be solved for each time epoch. Or, one can difference observations between the (more than 3) satellites and thus eliminate the common receiver clock error. Many geodetic receivers are capable of tracking the code and carrier signals on both L1 and L2 frequencies. This additional information allows solving for the linear ionospheric delay. It also helps in solving for the phase ambiguity. Differencing the observables with respect to those of another receiver (usually stationary) observing the same satellites yields only relative positions, but also reduces the satellite clock error and effects due to orbit error, as well as ionospheric and

tropospheric delays. It is worth mentioning that an INS also provides additional information, although it is only in the form of relative positions and introduces several additional systematic errors. Yet, with proper modeling, integrating INS into the GPS positioning problem solves difficulties in the kinematic mode related to achieving required resolution and accuracy and recovering from the inevitable cycle slips in the phase data.

We consider only the *double differencing* of pseudorange and phase observables from two receivers, one at a base station and the other on the vehicle. This eliminates receiver and satellite clock and phase biases (approximately). Two subscripts, r, s, are used to signify the between-receiver difference and two superscripts, p, q, are used to signify the between-satellite difference. We have a doubly differenced pseudorange and phase observable for each frequency, L1 and L2, thus four observables at each epoch, that can be combined in one observation set as follows:

$$\begin{pmatrix} \Delta s1_{r,s}^{p,q}(\tau) \\ \Delta s2_{r,s}^{p,q}(\tau) \\ \Delta \phi 1_{r,s}^{p,q}(\tau) \\ \Delta \phi 2_{r,s}^{p,q}(\tau) \end{pmatrix} = \begin{pmatrix} 1 & 1 & 0 & 0 \\ 1 & \alpha & 0 & 0 \\ 1/\lambda_1 & -1/\lambda_1 & -1 & 0 \\ 1/\lambda_2 & -\alpha/\lambda_2 & 0 & -1 \end{pmatrix} \begin{pmatrix} \Delta \rho_{r,s}^{p,q}(\tau) \\ \Delta I_{r,s}^{p,q} \\ \Delta N1_r^{p,q} \\ \Delta N2_r^{p,q} \end{pmatrix} + \begin{pmatrix} \Delta \varepsilon 1_{\rho,r,s}^{p,q} \\ \Delta \varepsilon 2_{\rho,r,s}^{p,q} \\ \Delta \varepsilon 1_{\phi,r,s}^{p,q} \\ \Delta \varepsilon 2_{\phi,r,s}^{p,q} \end{pmatrix} \tag{2.5}$$

where the wavelengths of the carrier signals are λ_1 and λ_2 (frequencies are f_1 and f_2), and where:

$$\Delta s1_{r,s}^{p,q}(\tau) = s1_r^p(\tau_r) - s1_r^q(\tau_r) - s1_s^p(\tau_s) + s1_s^q(\tau_s)$$

$$\Delta \phi 1_{r,s}^{p,q}(\tau) = \phi 1_r^p(\tau_r) - \phi 1_r^q(\tau_r) - \phi 1_s^p(\tau_s) + \phi 1_s^q(\tau_s)$$

$$\begin{aligned} \Delta \rho_{r,s}^{p,q}(\tau) = {} & \rho_r^p(\tau) - \rho_r^q(\tau) - \rho_s^p(\tau) + \rho_s^q(\tau) \\ & - c\left(\Delta\tau^p(t - \Delta t_r^p) - \Delta\tau^q(t - \Delta t_r^q) - \Delta\tau^p(t - \Delta t_s^p) + \Delta\tau^q(t - \Delta t_s^q)\right) \\ & - \left(\dot\rho_r^p - \dot\rho_r^q\right)\Delta\tau_r(t) + \left(\dot\rho_s^p - \dot\rho_s^q\right)\Delta\tau_s(t) \end{aligned} \tag{2.6}$$

$$\Delta I_{r,s}^{p,q} = I_r^p - I_r^q - I_s^p + I_s^q$$

$$\Delta N1_{r,s}^{p,q} = N1_r^p - N1_r^q - N1_s^p + N1_s^q$$

$$\Delta \varepsilon 1_{\rho,r,s}^{p,q} = \varepsilon 1_{\rho,r}^p - \varepsilon 1_{\rho,r}^q - \varepsilon 1_{\rho,s}^p + \varepsilon 1_{\rho,s}^q$$

and where it can be shown that the ionospheric term, I_r^p, is proportional to the pseudorange and phase delays as shown in the second column of the matrix in (2.5), with $\alpha = (f_1/f_2)^2$. Definitions similar to (2.6) hold for the second frequency, L2. The true ranges refer to different true times

since the receivers are not synchronized perfectly. In addition, the satellite clock errors do not cancel completely because they refer to different times of transmission.

Up to this point, the unknown parameter of primary interest was identified simply as the range; but the actual unknowns, of course, are the coordinates of the receiver. Toward determining these, one must examine the true range, for example, ρ_r^p, between the receiver and the p^{th} satellite. It is given, in terms of the true time of reception, explicitly by

$$\rho_r^p(t) = \left| R_3\left(\Delta t_r^p\, \omega_e\right) \mathbf{x}^p(t - \Delta t_r^p) - \mathbf{x}_r(t) \right| \tag{2.7}$$

where $\mathbf{x}^p(t - \Delta t_r^p)$ is the true vector of coordinates of the satellite at the true time of signal transmission and $\mathbf{x}_r(t)$ is the true vector of coordinates of the receiver at the true time of reception. The coordinates of these position vectors are in an Earth-centered-Earth-fixed system. That is why the satellite position vector must be prefixed with a rotation matrix that advances it by the angle $\Delta t_r^p\, \omega_e$ to the frame of the receiver at the time of reception, where ω_e is Earth's rate of rotation.

2.5 Estimation of Receiver Positions

In all cases, we will assume a linear model for the relationship between the unknowns and the observables. Also, only the double difference types of observations (2.5) will be considered. The cases where the relationship is non-linear, as for the unknown coordinates, $\mathbf{x}_r$, in (2.7), a linearization must be developed. Since usually the number of unknowns is smaller than the number of observations, a least-squares techniques based on minimizing the square of residuals between observation and adjusted observation is employed to find the optimal solution. It is noted, however, that the coordinates in the present context of kinematic positioning depend on time, and thus the number of parameters (coordinates of positions) is quite large, being at least three times the total number of epochs. This suggests a recursive linear least-squares approach, that is, the Kalman filter algorithm. This has the added benefit that parameters, or states, of the system may be added or deleted as time progresses and as warranted by the situation and with systematic and rigorous propagation of the covariances.

The Dynamics Model for the Unknowns. Following this approach, it is first necessary to identify the states of the system and to specify a model for their dynamics. Among the states one naturally includes the position coordinate errors; but also the velocity errors, the clock errors, and assorted perturbing effects due to atmosphere, multipath, and electronic delays may be included. For each state variables, one must define a (linear) dynamics model, with appropriate statistical information.

The simplest assumption is that the coordinate errors essentially are completely unknown, that is, they are states with arbitrarily large white noise. The dynamics model then loses its significance, and, lacking a better one at this point, we proceed under this assumption.

Let the state of the system be represented by the 3×1 vector, $\delta\mathbf{x}_k$. Here, the receiver subscript, r, has been omitted since only the coordinate errors of the roving receiver are to be estimated; while the subscript, k, refers to the time epoch. The "dynamics" of this state, as per above assumption, is

$$\delta\mathbf{x}_k = \mathbf{w}_k \tag{2.8}$$

where $\mathbf{w}_k$ is a 3×1 Gaussian (normally distributed) white noise vector with

$$\mathbf{w}_k \sim \mathcal{N}(0,Q_k) \tag{2.9}$$

and (in a qualitative sense) the covariance matrix of the noise is given by

$$Q_k = \begin{pmatrix} \infty & 0 & 0 \\ 0 & \infty & 0 \\ 0 & 0 & \infty \end{pmatrix} \tag{2.10}$$

The model (2.8) implies that the state transition matrix, Φ, is zero. The initial estimates of the states are also equal to zero. It is noted that the true position errors are the differences between the coordinates "indicated" by the system, in this case selected initial values, denoted by $\tilde{\mathbf{x}}_k$, and the true coordinates:

$$\delta\mathbf{x}_k = \tilde{\mathbf{x}}_k - \mathbf{x}_k \tag{2.11}$$

More sophisticated models for the coordinate errors would assume, for example, that the error at time k is correlated with the position error at time k+1, as described by a reasonable variance for the velocity error or acceleration error (see Leick, 1995). Lacking specific dynamics, the model (2.8) requires that adequate observations be available at every epoch in order to estimate the errors.

The Measurement Equations. The observations are the doubly differenced pseudoranges and phases for a number of satellites at each epoch. In practice the observations are processed in two passes. In the first pass, the equation (2.5) is used to solve for the double-difference cycle ambiguity for each observed combination of satellites. It turns out that the correlations of the estimated unknowns in (2.5) with the *difference* in L1 and L2 ambiguities are much less than with either ambiguity by itself (Leick, 1995). Therefore, the so-called wide-lane ambiguity

$$\Delta(N1 - N2)_{r,s}^{p,q} = \left(N1_r^p - N1_r^q - N1_s^p + N1_s^q\right) - \left(N2_r^p - N2_r^q - N2_s^p + N2_s^q\right) \tag{2.12}$$

is determined in the initial pass of the GPS data.

Subsequently, now that this parameter (the wide-lane ambiguity) is known, the only observation equation used is that of the "wide-lane phases":

$$\Delta(\phi 1 - \phi 2)_{r,s}^{p,q}\Big|_k = \left(\phi 1_r^p - \phi 1_r^q - \phi 1_s^p + \phi 1_s^q\right)_k - \left(\phi 2_r^p - \phi 2_r^q - \phi 2_s^p + \phi 2_s^q\right)_k \tag{2.13}$$

which is related to the unknown coordinates of the receiver according to (2.4) by

$$\Delta(\phi 1 - \phi 2)^{p,q}_{r,s}\Big|_k = \frac{f_{01} - f_{02}}{c}\left(\rho^p_r - \rho^q_r - \rho^p_s + \rho^q_s\right)_k - \Delta(N1 - N2)^{p,q}_{r,s} + \Delta(\varepsilon 1 - \varepsilon 2)^{p,q}_{\phi,r,s}\Big|_k \tag{2.14}$$

where the ranges are given by (2.7).

At any particular epoch, the measurement equation relates the 3 states, $\delta\mathbf{x}_k$, to n differences between observed quantities of the type (2.14) and corresponding calculated quantities. Let $\mathbf{y}_k$ be the $n \times 1$ vector of observations at epoch k of the corresponding true function, $\mathbf{h}(\mathbf{x}_k)$, of the true parameters, presumably with additive discrete white noise:

$$\mathbf{y}_k = \mathbf{h}(\mathbf{x}_k) + \mathbf{v}_k \tag{2.15}$$

The difference between the vectors of calculated values and observations is given by

$$\begin{aligned} \delta\mathbf{y}_k &= \mathbf{h}(\tilde{\mathbf{x}}_k) - \mathbf{y}_k \\ &= \tilde{\mathbf{y}}_k - \mathbf{y}_k \end{aligned} \tag{2.16}$$

A linear approximation of $\delta\mathbf{y}_k$ is given by

$$\begin{aligned} \delta\mathbf{y}_k &= \mathbf{h}(\tilde{\mathbf{x}}_k) - \mathbf{h}(\mathbf{x}_k) - \mathbf{v}_k \\ &\approx \mathrm{H}_k\,\delta\mathbf{x}_k - \mathbf{v}_k \end{aligned} \tag{2.17}$$

where

$$\mathrm{H}_k = \frac{\partial \mathbf{h}}{\partial \mathbf{x}}\Big|_{\mathbf{x} = \bar{\mathbf{x}}_k} \tag{2.18}$$

is a $n \times 3$ matrix of evaluated partial derivatives.

In the present case,

$$\delta\mathbf{y}_k = \left[\Delta(\tilde{\phi}1 - \tilde{\phi}2)^{p,q}_{r,s}\Big|_k - \Delta(\phi 1 - \phi 2)^{p,q}_{r,s}\Big|_k\right]_{(p,q) \in Z} \quad ; \quad n \times 1 \text{ vector} \tag{2.19}$$

where Z is the set of integer pairs designating the two satellites that enter in the calculation of a double difference observation (Z contains n such pairs), and where

$$\Delta(\tilde{\phi}1 - \tilde{\phi}2)^{p,q}_{r,s}\Big|_k = \frac{f_{01} - f_{02}}{c}\left(\tilde{\rho}^p_r - \tilde{\rho}^q_r - \tilde{\rho}^p_s + \tilde{\rho}^q_s\right)_k - \Delta(N1 - N2)^{p,q}_{r,s} \tag{2.20}$$

is the double difference phase at epoch k computed on the basis of the approximate roving receiver coordinates, $\tilde{\mathbf{x}}_k$ (the subscript, r, has been deleted for the sake of convenience). The ranges $\tilde{\rho}_s^p$ and $\tilde{\rho}_s^q$ are computed according to (2.7) for each epoch using the given coordinates of the stationary receiver and the coordinates of the satellites p and q. The corresponding ranges to the roving receiver are computed from

$$\tilde{\rho}_r^p\Big|_k = \left| R_3\left(\Delta t_r^p\, \omega_e\right) \mathbf{x}^p(t - \Delta t_r^p) - \tilde{\mathbf{x}}_k \right| \tag{2.21}$$

and similarly for $\tilde{\rho}_r^q$.

The $n \times 3$ measurement matrix of partial derivatives in (2.18) for each epoch, k, is given by

$$\mathbf{H}_k = \left[-\frac{1}{\tilde{\rho}_k^p}\left[R_3\left(\Delta t_k^p\, \omega_e\right) \mathbf{x}^p(\tau_k - \Delta t_k^p) - \tilde{\mathbf{x}}_k \right]^T + \frac{1}{\tilde{\rho}_k^q}\left[R_3\left(\Delta t_k^q\, \omega_e\right) \mathbf{x}^q(\tau_k - \Delta t_k^q) - \tilde{\mathbf{x}}_k \right]^T \right]_{(p,q) \in Z} \tag{2.22}$$

where, again, the subscript, r, has been omitted. Finally, the white noise vector in (2.17) is

$$\mathbf{v}_k = \left[\Delta(\varepsilon 1 - \varepsilon 2)_{\phi,r,s}^{p,q}\Big|_k \right]_{(p,q) \in Z} \quad ; \quad n \times 1 \text{ vector} \tag{2.23}$$

In the calculation of the ranges $\tilde{\rho}_s^p$, $\tilde{\rho}_s^q$, $\tilde{\rho}_r^q$, and $\tilde{\rho}_s^p$, as well as the matrix $\mathbf{H}_k$, the signal transit times, like Δt_r^p, can be calculated from approximate receiver and satellite positions.

The covariance matrix, $\mathbf{R}_k$, of the measurement noise vector, $\mathbf{v}_k$, at epoch k, is determined by appropriate transformation from the covariance matrix of the phase observations (i.e., taking due account of the covariance propagation associated with the double differencing). It is assumed that the errors from epoch to epoch are uncorrelated.

Under these simplifying assumptions (no dynamics model for the position errors, no correlation of observation errors in time), the position error states are estimated epoch by epoch using the standard least-squares solution:

$$\delta\hat{\mathbf{x}}_k = -\left(\mathbf{H}_k^T \mathbf{R}_k^{-1} \mathbf{H}_k\right)^{-1} \mathbf{H}_k^T \mathbf{R}_k^{-1}\, \delta\mathbf{y}_k \tag{2.24}$$

with covariance matrix given by

$$\mathbf{P}_k = \left(\mathbf{H}_k^T \mathbf{R}_k^{-1} \mathbf{H}_k\right)^{-1} \tag{2.25}$$

From (2.11), the estimated coordinates of the GPS receiver at epoch k are given by

$$\hat{\mathbf{x}}_k = \tilde{\mathbf{x}}_k - \delta\mathbf{x}_k \tag{2.26}$$

These Cartesian Earth-Centered-Earth-fixed coordinates can be converted to geodetic latitude, longitude, and height (e.g., with respect to the Geodetic Reference System 1980) using standard formulas (Borkowski, 1989).

CHAPTER 3

THE INERTIAL NAVIGATION SYSTEM

3.1 Introduction

An inertial navigation system (INS) consists of an inertial measurement unit (IMU) and a navigation computer. The essential element of an IMU is the accelerometer whose output is integrated twice in time to obtain positions. A common class of accelerometers is the force-rebalance type. Although a variety of designs exist, most are based on the principle of maintaining the null position of a proof mass on a spring. The electronically applied force needed to do this is a measure of the acceleration. Three accelerometers with sensitive axes mutually perpendicular provide three-dimensional navigation.

Of equal importance, however, is the coordinate frame in which the accelerometers are to provide positions. In this respect, not only the orientation of the accelerometers in the coordinate system, but also their angular velocity affect the determination of position. The orientation determines the component of the position vector that a particular accelerometer provides; and, as is known from elementary physics, the angular rates with respect to an inertial frame contaminate the accelerometer outputs with centrifugal and Coriolis accelerations.

The orientation and angular rates of the accelerometer platform are determined with gyroscopes. Most INS for commercial deployment, today, use either the *ring laser gyro* or the less costly (and less accurate) fiber optic gyro. Both types of gyros require that the INS be mechanized in the so-called *strapdown* configuration; that is the INS is physically mounted to the frame of the vehicle (no gimbal support system). This reduces the cost of the INS considerably as compared to gimbal-supported, local-level stabilized systems.

3.2 The Ring Laser Gyro

The ring laser gyro (RLG), in principle, has no moving parts - it is based on the concept of the Sagnac effect: The frequency of a light beam travelling in a resonant closed circuitous path (where the number of wavelengths is always the same; i.e., it is a laser) must change if the *apparent* length of the circuit changes because it rotates in inertial space. Two such counter-travelling beams of light are used to create a fringe pattern where they recombine. The fringe pattern is stationary if there is no rotation in inertial space. But, it migrates in the presence of rotation about the axis perpendicular to the plane of the circuit, because then one beam sees a longer path, the other a shorter path; and the number of fringes passing a detector per unit time indicates the rate of rotation.

The major problem with RLG's is a phenomenon called lock-in: due to imperfections (scattering of light in the resonant cavity) the two beams lase at the same frequency even in the presence of a small rotation, typically up to several hundred degrees per hour; they lock to the same frequency and indicate a zero rotation. One common solution to this problem is to bias the output of the device by applying a physical rotation away from the lock-in range. To maintain stability, this mechanical "bias" is in the form of an alternating rotation, i.e., a dithering or oscillation (tens

to hundreds of Hz) of the gyro about its sensitive axis. This is the operational concept of the gyros used in the Litton LN93 INS.

A newer approach is to apply an optical bias by creating left- and right-circular polarization of the two beams, respectively. In the presence of an applied magnetic field, the speeds of the beams differ, which is equivalent to an effective difference in path length (Faraday effect), hence creating a bias in the frequency difference. The complete absence of moving parts (no mechanical dithering) improves the stability and substantially reduces the random noise of the IMU as a whole. This is the operational concept of the gyros used in the Litton LN100 INS.

3.3 Essential INS Characteristics and Configuration

Size, weight, and power requirements, as well as the standard error budgets for each system are listed in Tables 3.1 and 3.2. The accelerometers are the same model for both systems, but current sensors are slightly improved. The characteristics of these two systems were provided by Litton (person communication). Both are quite similar and several other subordinate error sources, especially misalignments, temperature transients, and other correlated noise, as well as acceleration sensitivities are not included here.

Table 3.1: Essential characteristics of the LN93 and LN100 inertial systems.

	LN93	LN100
Data Rate	20 Hz (user defined)	32 Hz (256 Hz, raw data)
Size (excludes mount)	1089 cu. in.	539 cu. in.
Weight (excludes mount)	48.5 lbs.	19.4 lbs
Power	28 VDC, 150 Watts	28 VDC, 26.5 Watts

Table 3.2: Essential error budget for LN93 and LN100 inertial systems.

	LN93	LN100
Accelerometer (Litton A-4 model)		
Bias Error	25 mGal	20 mGal
Scale Factor Error	120 ppm	40 ppm
White Noise	5 mGal/$\sqrt{Hz}$	5 mGal/$\sqrt{Hz}$
Gyro (ring laser gyro)		
Bias (Drift) Error	0.003 °/hr	0.003 °/hr
Scale Factor Error	5 ppm	0.2 ppm
White Noise	0.0015 °/$\sqrt{hr}$	< 0.001 °/$\sqrt{hr}$

Figure 3.1 shows the basic configuration of the INS and computer interface for the LN93. A similar setup exists for the LN100. The computer used with the LN93 is a laptop computer mounted in a so-called docking station that contains both the 1553 bus controller card and the timer card. The 1553 card is the direct interface to the INS and all requests of data from the INS are made through this bus controller. The timer card can be programmed to synthesize a sequence of interrupts at a specified rate which is then used to request the INS data at that rate. In the case of the LN93, the data request rate is 20 Hz. The start of a sequence of 20 interrupts within each second is initiated by the pulse coming from the GPS receiver that is synchronized to GPS time within a millisecond, or better, depending on the receiver. This pulse also is used to reset the INS clock to zero. Thus all INS data requests are synchronized to GPS time. Each data item from the INS includes a time validity tag relative to the INS clock which can be used to determine the actual time for which the data item corresponds. Additional data are retrieved from the GPS receiver by the bus controller software to determined the actual GPS time stamp of the one-second-pulse, and to provide altitude data for the INS. The INS data are saved by the bus controller software on the hard disk storage device of the laptop computer. The GPS raw data are stored in the GPS receiver and later retrieved and processed as described in Chapter 2.

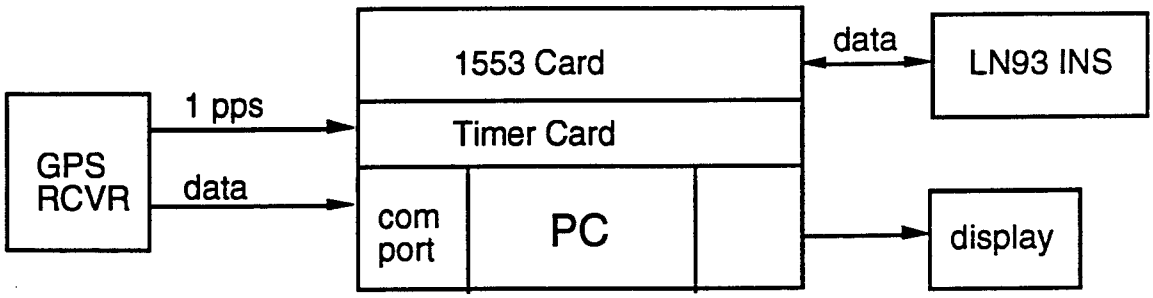

Figure 3.1: Basic configuration of INS, GPS receiver, and computer test equipment.

3.4 INS Data Output

The data output options of an INS range from position and velocity to orientation angles, as well as raw sensor data, system status data, and time tags. The type of output is entirely dictated by the navigation software that the INS manufacturer creates for its customers. The software for the LN93, that is on loan to Ohio State University from Litton, allows users to request position and velocity in the navigation frame (north, east, down; or NED) with double precision (32 bit data) and orientation angles of the body frame with respect to the navigation frame in single precision (16 bit data). The position coordinates have quantization errors of about 40 cm in latitude and 60 cm in longitude, being due entirely to an artifact of the data processing performed by the navigation software. The velocities do not have this error and can be integrated independent of the INS software to obtain very precise position coordinates at the millimeter level.

Nevertheless, the lack of availability of raw sensor data from the LN93 makes it less useful for wider geodetic applications. In addition, care must be exercised in synchronizing the INS and GPS data, since the INS software, performing real-time data processing, makes data available to the user with time validity tags showing significant time delays from the actual data output time.

The software of the LN100 obtained by OSU's Center for Mapping was specifically modified to provide raw sensor data which can be processed by the user independently of the navigation software. Furthermore, the time synchronization is less problematic since the time of raw sensor output coincides very closely to the time validity of the data (since very little processing takes place).

The raw data comprise velocity increments, $\delta\mathbf{v}$, from the accelerometers and gyro angle increments, $\delta\boldsymbol{\theta}$, in vector form given by

$$\delta\mathbf{v} = \int_{\delta t} \mathbf{a}^b(t)\, dt \ , \quad \delta\boldsymbol{\theta} = \int_{\delta t} \boldsymbol{\omega}_{ib}^b(t)\, dt \tag{3.1}$$

where δt is the sampling interval (e.g., 1/256 s), $\mathbf{a}^b$ is the acceleration vector of the INS in the frame of the vehicle (the body frame, or b-frame), and $\boldsymbol{\omega}_{ib}^b$ is the angular rate of rotation of the vehicle (or, body) with respect to the inertial frame, as coordinatized in the body frame. Here we assume that the body frame and actual INS platform frame are identical (i.e., the axes of the INS, being strapped down, are parallel to the principal axes of the aircraft: forward, to the right, and through the floor).

The set of INS navigation equations implemented by the INS navigation computer are differential equations of velocity and position, where the velocity part may be formulated generally as

$$\begin{aligned} \dot{v}_N &= a_N + f_N(\mathbf{v},h,\phi) \\ \dot{v}_E &= a_E + f_E(\mathbf{v},h,\phi) \end{aligned} \tag{3.2}$$

where $\mathbf{v} = \left(v_N, v_E, v_D\right)^T$ is the velocity vector in the navigation frame with north, east, and down components, $\mathbf{a}^n = \left(a_N, a_E, a_D\right)^T$ is the acceleration vector in the same frame, h is height above a reference ellipsoid, ϕ is geodetic latitude, and f_N, f_E are known functions. These navigation equations are integrated to obtain velocities, which are further integrated to obtain positions. The navigation-frame accelerations are determined from the body-frame accelerations using a rotation matrix, C_b^n:

$$\mathbf{a}^n = C_b^n\, \mathbf{a}^b \tag{3.3}$$

The rotation matrix, C_b^n, is determined from the gyro angles by integrating the following differential equation:

$$\dot{C}_b^n = C_b^n \left[\boldsymbol{\omega}_{nb}^b \times\right] \tag{3.4}$$

where with $\boldsymbol{\omega}_{nb}^b = \left(\omega_1, \omega_2, \omega_3\right)^T$ we define

$$\left[\boldsymbol{\omega}_{nb}^{b}\times\right]=\begin{pmatrix} 0 & -\omega_3 & \omega_2 \\ \omega_3 & 0 & -\omega_1 \\ -\omega_2 & \omega_1 & 0 \end{pmatrix} \tag{3.5}$$

It remains to determine the angular rates, $\boldsymbol{\omega}_{nb}^{b}$, of the body frame with respect to the navigation frame; and this is accomplished with the relationship

$$\boldsymbol{\omega}_{nb}^{b} = \boldsymbol{\omega}_{ib}^{b} - C_{n}^{b}\,\boldsymbol{\omega}_{in}^{n} \tag{3.6}$$

where the inertial rates, $\boldsymbol{\omega}_{ib}^{b}$, of the body are obtained from the gyros according to (3.1), and the inertial rates of the navigation frame, $\boldsymbol{\omega}_{in}^{n}$, are obtained from the velocities.

Clearly, the navigation solution as outlined above involves a rather complicated numerical procedure, the elaboration of which is beyond the scope of this report (see Jekeli, 1996a). The final output data processed by the INS computer consist of geodetic latitude and longitude, as well as orientation angles, being defined as roll, pitch, and yaw angles of the vehicle with respect to the north, east, and down directions. The height of the vehicle cannot be determined from the INS because of the well known vertical instability of the navigation solution due to the Earth's centrally directed gravitational acceleration.

CHAPTER 4

POSITION ESTIMATION

4.1 Introduction

The integration of the two systems, GPS and INS, means primarily a fusion of the data from each system in order to obtain the (best) position of the platform or vehicle at any time. Mathematically, one may view the problem as presented in Sections 2.6 and 2.7. The position coordinate errors are states (unknown parameters) that are measured via the measurement equation (2.15). The states, themselves, are assumed to behave according to some dynamics model. In the case of GPS alone, the simplest model is given by (2.8), namely that the states unless measured by GPS are completely unknown. Other models might include some information about the velocity of the vehicle, etc., in order to predict what the states might be just before a new GPS measurement. In particular the incorporation of an INS provides very significant information on how the states behave between GPS measurements since, in fact, the INS senses accelerations that precisely indicate how the position of the vehicle varies in time.

4.2 System Error Dynamics

The model for the INS position error states is well known and can be derived from the navigation equations and ancillary equations (3.2) through (3.6). The development of the system error dynamics in the n-frame is found in great detail in the book by Britting (1971); see also (Jekeli, 1996a). We give here only the formulas without derivation.

The states include not only position and velocity errors, but also orientation angles, since all three types of errors are highly coupled. Let this vector of error states be

$$\boldsymbol{\varepsilon}_1 = \left(\psi_N \;\; \psi_E \;\; \psi_D \;\; \delta\dot{\phi} \;\; \delta\dot{\lambda} \;\; \delta\dot{h} \;\; \delta\phi \;\; \delta\lambda \;\; \delta h \right)^T \tag{4.1}$$

where ψ_N, ψ_E, ψ_D are the errors in roll, pitch, and yaw angles, respectively, and the errors in velocity and position are given in terms of latitude, ϕ, longitude, λ, and height, h. Then the dynamics of this state vector are defined by the following linear differential equation:

$$\frac{d}{dt}\boldsymbol{\varepsilon}_1 = F_1 \boldsymbol{\varepsilon}_1 + G\,\delta\mathbf{u} \tag{4.2}$$

where, with $r = R_\phi + h$, $\ell_1 = \dot{\lambda} + \omega_e$, and $\ell_2 = \dot{\lambda} + 2\,\omega_e$, R_ϕ being the Earth's meridian radius of curvature at geodetic latitude, ϕ, and ω_e being Earth's rate of rotation, we have

$F_1 =$

$$\begin{bmatrix}
0 & -\dot{\ell}_1\sin\phi & \dot{\phi} & 0 & \cos\phi & 0 & -\dot{\ell}_1\sin\phi & 0 & 0 \\
\dot{\ell}_1\sin\phi & 0 & \ell_1\cos\phi & -1 & 0 & 0 & 0 & 0 & 0 \\
-\dot{\phi} & -\dot{\ell}_1\cos\phi & 0 & 0 & -\sin\phi & 0 & -\dot{\ell}_1\cos\phi & 0 & 0 \\
0 & \frac{-a_3^n}{r} & \frac{a_2^n}{r} & \frac{-2\dot{h}}{r} & -\dot{\ell}_1\sin 2\phi & \frac{-2\dot{\phi}}{r} & -\dot{\lambda}\ell_2\cos 2\phi & 0 & \frac{\ddot{\phi}+\frac{1}{2}\dot{\lambda}\ell_2\sin 2\phi}{-r} \\
\frac{a_3^n}{r\cos\phi} & 0 & \frac{-a_1^n}{r\cos\phi} & 2\dot{\ell}_1\tan\phi & 2\left(\dot{\phi}\tan\phi-\frac{\dot{h}}{r}\right) & \frac{-2\dot{\ell}_1}{r} & \begin{matrix}2\dot{\ell}_1\left(\dot{\phi}+\frac{\dot{h}\tan\phi}{r}\right)\\ +\ddot{\lambda}\tan\phi\end{matrix} & 0 & \frac{2\dot{\phi}\dot{\ell}_1\tan\phi-\ddot{\lambda}}{r} \\
a_2^n & -a_1^n & 0 & 2r\dot{\phi} & 2r\dot{\ell}_1\cos^2\phi & 0 & -r\dot{\lambda}\ell_2\sin 2\phi & 0 & \dot{\phi}^2+\dot{\lambda}\ell_2\cos^2\phi \\
0 & 0 & 0 & 1 & 0 & 0 & 0 & 0 & 0 \\
0 & 0 & 0 & 0 & 1 & 0 & 0 & 0 & 0 \\
0 & 0 & 0 & 0 & 0 & 1 & 0 & 0 & 0
\end{bmatrix} \tag{4.3}$$

and where

$$G=\begin{pmatrix} -C_b^n & 0 & 0 \\ 0 & D^{-1}C_b^n & D^{-1} \\ 0 & 0 & 0 \end{pmatrix}; \quad D=\begin{pmatrix} R_\phi+h & 0 & 0 \\ 0 & (R_\phi+h)\cos\phi & 0 \\ 0 & 0 & -1 \end{pmatrix} \tag{4.4}$$

and the inputs that drive the error dynamics are the gyro errors, $\delta\boldsymbol{\omega}_{ib}^b$, the accelerometer errors, $\delta\mathbf{a}^b$, both in the body frame, and the disturbing gravitational vector, $\delta\mathbf{g}^n$, in the n-frame:

$$\delta\mathbf{u}=\begin{pmatrix} \delta\boldsymbol{\omega}_{ib}^b \\ \delta\mathbf{a}^b \\ \delta\mathbf{g}^n \end{pmatrix} \tag{4.5}$$

The instrument errors consist of biases, scale factor errors, correlated noise, and white noise. This fact introduces an additional set of models that characterize the dynamic behavior of these errors. Also, the gravitational error may be modeled as a stochastic process, which requires another model. In total then, the simple nine-state error dynamics model (4.2) must be extended to include models for the disturbances (4.5).

4.3 Instrument Error and Gravity Field Models

The errors of the accelerometers and the gyros in the body frame can be modeled in a variety of ways, but usually the models are restricted to linear processes. That is, an error is described by a linear differential equation with white noise forcing function. For example, the process, x, is assumed to have a first-order Gauss-Markov model if:

$$\dot{x} = -\beta x + w \tag{4.6}$$

where w is a zero-mean, Gaussian (normally distributed), random number. This yields a stochastic description of the process, x, in terms of its variance, σ^2, and a correlation time, $1/\beta$. The spectral density of w in (4.6) is the constant, $2\beta\sigma^2$. If the correlation time is assumed to be infinite (but the spectral density of the white noise is nonzero), then the process is a random walk; if further the white noise is zero, then x is a random bias.

In accordance with Table 3.2, the accelerometer and gyro errors, respectively, are decomposed into bias errors, $\mathbf{b}$ and $\mathbf{d}$, white noise, $\mathbf{w}_a$ and $\mathbf{w}_g$, accelerometer scale factor error, κ_a, and accelerometer colored noise, ν_a. The latter (not listed in Table 3.2), assumed to be of the form (4.6) with standard deviation of 5 mGal and correlation time of 10 minutes, was included since a model for it was available from the manufacturer specifications. On the other hand, the gyro scale factor error is too small to have any consequence, and therefore, was excluded. The total inertial instrument errors are represented as follows (each vector contains corresponding components for each of the three respective sensors):

$$\begin{aligned} \delta\mathbf{a}^b &= \mathbf{b} + [\mathbf{a}^b\cdot]\boldsymbol{\kappa}_a + \boldsymbol{\nu}_a + \mathbf{w}_a \\ \delta\boldsymbol{\omega}_{ib}^b &= \mathbf{d} + \mathbf{w}_g \end{aligned} \tag{4.7}$$

where $[\mathbf{a}^b\cdot]$ denotes a diagonal matrix with the components of $\mathbf{a}^b$ as diagonal elements. The colored noise is assumed to be of the form (4.6), while the bias and scale factor errors are assumed to be unknown constants with a given variance and are defined to be states of the system:

$$\boldsymbol{\varepsilon}_2 = \begin{bmatrix} \mathbf{d} \\ \mathbf{b} \\ \boldsymbol{\kappa}_a \\ \boldsymbol{\nu}_a \end{bmatrix} \tag{4.8}$$

As such these states are incorporated into the dynamics of the system through the following differential equations:

$$\dot{\varepsilon}_2 = \begin{bmatrix} 0 \\ 0 \\ 0 \\ -[\beta_{a\cdot}]\,\nu_a + w_\nu \end{bmatrix} \tag{4.9}$$

The unknown gravitation, $\delta\bar{g}^n$, known as the gravity disturbance vector, can also be modeled as a stochastic process (Moritz, 1980). The degree to which the disturbance must be modeled in this way depends on the *reference* gravitational model already available. Today, the gravity field is known quite well, generally to a few parts per million. The third-order Gauss-Markov model of (Jekeli, 1994) was chosen:

$$\dot{\varepsilon}_3 = B\varepsilon_3 + w_3\,; \quad \delta\bar{g}^n = A\,\varepsilon_3 \tag{4.10}$$

where the states ε_3 are driven (or forced) by the white noise, w_3 (in this form, as a vector first-order differential equation, only the last three elements of the white noise vector are non-zero). Matrices A and B depend on the order of the Gauss-Markov model.

4.4 The State-Space Model

Combining (4.5), (4.7), and (4.10) yields

$$\delta u = \begin{bmatrix} I & 0 & 0 & 0 & 0 \\ 0 & I & [a^b\cdot] & I & 0 \\ 0 & 0 & 0 & 0 & A \end{bmatrix} \begin{bmatrix} d \\ b \\ \kappa_a \\ \nu_a \\ \varepsilon_3 \end{bmatrix} + \begin{bmatrix} w_g \\ w_a \\ 0 \end{bmatrix} \tag{4.11}$$

where I is a 3×3 identity matrix and 0 is a 3×3 zero matrix. Substituting (4.11) into (4.2) and augmenting with (4.9) and (4.10) then yields the total system of state equations:

$$\frac{d}{dt}\begin{bmatrix} \varepsilon_1 \\ {\scriptstyle 9x1} \\ \varepsilon_2 \\ {\scriptstyle 12x1} \\ \varepsilon_3 \\ {\scriptstyle 9x1} \end{bmatrix} = \begin{bmatrix} F_{11} & F_{12} & F_{13} \\ {\scriptstyle 9x9} & {\scriptstyle 9x12} & {\scriptstyle 9x9} \\ 0 & F_{22} & 0 \\ {\scriptstyle 12x9} & {\scriptstyle 12x12} & {\scriptstyle 12x9} \\ 0 & 0 & B \\ {\scriptstyle 9x9} & {\scriptstyle 9x12} & {\scriptstyle 9x9} \end{bmatrix} \begin{bmatrix} \varepsilon_1 \\ {\scriptstyle 9x1} \\ \varepsilon_2 \\ {\scriptstyle 12x1} \\ \varepsilon_3 \\ {\scriptstyle 9x1} \end{bmatrix} + \begin{bmatrix} G_1 \\ {\scriptstyle 9x18} \\ G_2 \\ {\scriptstyle 12x18} \\ G_3 \\ {\scriptstyle 9x18} \end{bmatrix} \begin{bmatrix} w_g \\ {\scriptstyle 3x1} \\ w_a \\ {\scriptstyle 3x1} \\ w_\nu \\ {\scriptstyle 3x1} \\ w_3 \\ {\scriptstyle 9x1} \end{bmatrix} \tag{4.12}$$

where the dimensions of each matrix and vector are indicated and a third-order Gauss-Markov model for the gravity disturbance is assumed. From (4.2), (4.4), and (4.11)

$$F_{11} = F_1 \; ; \quad F_{12} = \begin{bmatrix} -C_b^n & 0 & 0 & 0 \\ 0 & D^{-1} C_b^n & D^{-1} C_b^n [\mathbf{a}^b \cdot] & D^{-1} C_b^n \\ 0 & 0 & 0 & 0 \end{bmatrix} \; ; \quad F_{13} = \begin{bmatrix} 0 \\ 3x9 \\ D^{-1} A \\ 0 \\ 3x9 \end{bmatrix} \tag{4.13}$$

and similarly, from (4.9)

$$F_{22} = \begin{bmatrix} 0 & 0 & 0 & 0 \\ 0 & 0 & 0 & 0 \\ 0 & 0 & 0 & 0 \\ 0 & 0 & 0 & -[\beta_{\alpha} \cdot] \end{bmatrix} \tag{4.14}$$

Also, from (4.2) and (4.11)

$$G_1 = \begin{bmatrix} -C_b^n & 0 & 0_{3x15} \\ 0 & D^{-1} C_b^n & 0_{3x15} \\ 0 & 0 & 0_{3x15} \end{bmatrix} \tag{4.15}$$

and G_2, G_3 can be inferred from (4.9) and (4.10). The set of differential equations (4.12) describes the total dynamics of the various errors (including the unknown gravity disturbance) of the inertial system. It is certainly only a model - in the first place a linearization and in the second place an approximation as regards the white noise forcing function and the characterizations of the instrument errors and gravity disturbance components.

The noise processes $\mathbf{w}_a$, $\mathbf{w}_g$, $\mathbf{w}_v$, and $\mathbf{w}_3$ (equation 4.12) are independently and normally distributed with zero mean and standard deviations σ_a, σ_g, σ_v, and σ_3, respectively. These are approximated as being theoretically pure white noise processes with correlation functions

$$\mathcal{E}[w(t)w(t')] = \zeta^2 \delta(t-t') \tag{4.16}$$

where δ is the Dirac delta "function" and ζ^2 is the power spectral density (a constant) of the white noise process (values of ζ are listed in Table 3.2 for the first two white noise processes and $\zeta_v = 0.3$ mGal/s/$\sqrt{\text{Hz}}$; see (Jekeli, 1994) for the gravity disturbance model). The relationship between the psd of the white noise and the variance can be obtained by approximating the correlation (4.16) as a first-order Gauss-Markov process with short correlation time (say, less than the sampling interval). A typical relationship is

$$\zeta^2 = 2 \Delta t \, \sigma^2 \tag{4.17}$$

however, a more conservative relationship (less correlation at Δt) would omit the factor of 2. In the present case the white noise components of the instruments are specified in terms of the psd, and so (4.17) is not needed, but can be used to get the equivalent variance assuming the noise is white for all frequencies.

4.5 GPS/INS Integration

The type of GPS/INS integration considered for these studies is known as loose, or decentralized integration. In this mode, the data from each system are processed separately (and optimally) and then combined, in some fashion, to obtain the final position estimates. The individual processing schemes for GPS and INS have been outlined respectively in Chapters 2 and 3, above. Thus, the input to our integration scheme constitutes a set of positions derived from the GPS data and another set of positions provided by the INS. The alternative would be a centralized integration where the raw data of each system are processed simultaneously to obtain the optimal position estimates. Though perhaps preferable from an operational standpoint, this mode requires considerable more program development and is outside the scope of this project. On the other hand, decentralization also has its advantages, being generally more stable and allowing for better detection and isolation (and correction) of system failures.

There are varying degrees of loose integration, ranging from basically uncoupled integration to a coupling that adheres to the philosophy of the INS output yielding a dynamic behavior of the position error states. In other words, instead of knowing nothing about the errors in position between GPS epochs, the INS output allows us to interpolate what those errors might be on the basis of sensed acceleration. Clearly, the Kalman filter is the ideal processing tool in this case. Figures 4.1 and 4.2 show schematically the two loose integration options.

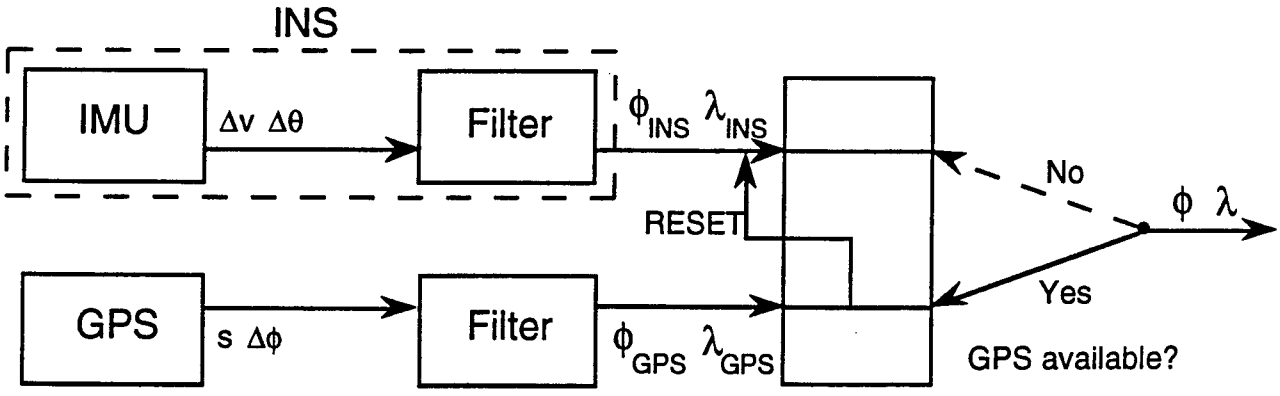

Figure 4.1. Uncoupled GPS/INS Integration

In the uncoupled integration mode, as depicted in Figure 4.1, the GPS positions are the final product on the right side unless they are unavailable. In the case that GPS positioning is lost, the INS position coordinates are reset to the GPS-derived coordinates at the time they are last available. From that time forward the INS is allowed to navigate and it provides the positions of the vehicle until GPS positioning resumes. The INS navigation is done without attempt to estimate any of its errors, whose calibrations were last done during the initialization of the system (usually at the start of the mission).

In the loosely coupled integration of GPS and INS, as depicted in Figure 4.2, an attempt is made to calibrate (estimate) the errors of the system using the GPS position data while they are available. This is done through the Kalman filter and smoother algorithms described below.

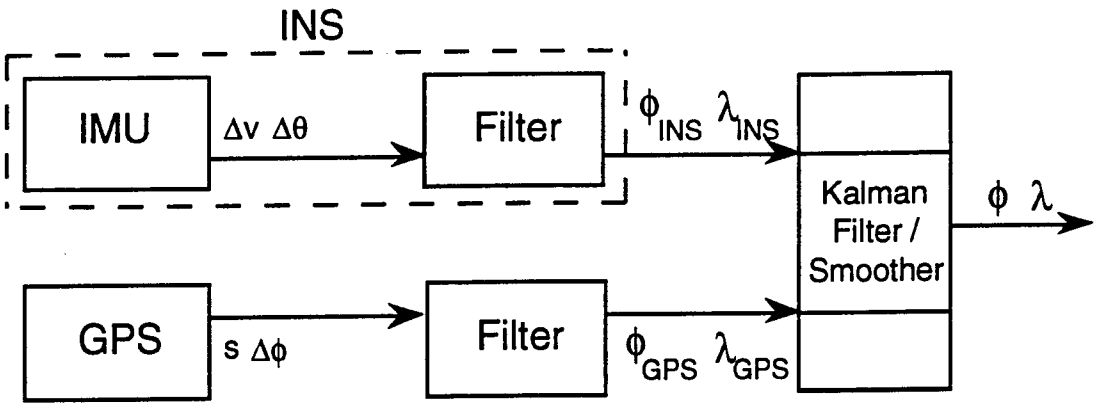

Figure 4.2. Loosely coupled GPS/INS Integration.

4.6 Discrete Kalman-Bucy Filtering

The conventional discrete Kalman-Bucy filter, to which the smoothing algorithm is closely related, is briefly summarized here. More details may be found in (Gelb, 1974). Instead of the simplistic model for the position errors, as exemplified by (2.8), the INS now gives very significant additional information on the errors, whose dynamics (as part of a larger set of error states associated with the INS) are given by the set of differential equations (4.12), which are repeated using simplified notation as indicated:

$$\dot{\delta x} = F\,\delta x + Gw \tag{4.18}$$

The reader will forgive the ambivalence in notation here, where for GPS the position coordinates are Cartesian, while for the INS the coordinates are the geodetic latitude, longitude, and height. As one set can be transformed easily into the other set, the lack of notational uniformity, while detracting in practical value, should not cause conceptual difficulties. The discrete equivalent of (4.18) is given by

$$\delta x_k = \Phi(t_k,t_{k-1})\,\delta x_{k-1} + G_{k-1}w_{k-1} \tag{4.19}$$

where Φ is the state transition matrix and w_{k-1} is the white noise sequence corresponding to the continuous white noise process w (Brown, 1983, p.254).

At specified intervals, denoted by index k, the states are measured. The optimal imposition of these measurements onto the dynamics of the system is done through the Kalman filter. The model for the measurements is given, as before, by (2.17):

$$\delta y_k = H_k\,\delta x_k - v_k \tag{4.20}$$

where H_k is a matrix whose elements are zero except those elements corresponding to the measured states (position errors) of δx_k, in which case they are equal to one (again, assuming like coordinates for both systems). v_k is a vector of observation errors presumably uncorrelated in time.

The Kalman filter algorithm proceeds as follows (Gelb, 1974). The state vector estimates propagate according to

$$\delta\hat{x}_k^- = \Phi(t_k,t_{k-1})\,\delta\hat{x}_{k-1} \tag{4.21}$$

from time t_{k-1} to the time just prior to the measurement update, t_k, (denoted by the superscript −). Initial values usually are taken as $\delta\hat{x}_0 = 0$. At the time, t_k, the estimate is improved due to the measurement according to

$$\delta\hat{x}_k = \delta\hat{x}_k^- + K_k\,(\delta y_k - H_k\,\delta\hat{x}_k^-) \tag{4.22}$$

where the "Kalman gain" is

$$K_k = P_k^- H^T (H\,P_k^- H^T + R_k)^{-1}; \qquad R_k = \mathcal{E}(v_k v_k^T) \tag{4.23}$$

The covariance matrix, P_k^-, is the propagated covariance from the time t_{k-1}. Let P_{k-1} denote the error covariance matrix of the estimated states at time t_{k-1}. At time t_k, prior to incorporation of the measurement, δy_k, the error covariance matrix has transitioned, due to the system dynamics, to

$$P_k^- = \Phi_{k,k-1}\,P_{k-1}\,\Phi_{k,k-1}^T + Q_{k-1} \tag{4.24}$$

where Q_{k-1} is the covariance matrix associated with the second term on the right side of (4.19). An initial covariance, P_0, has to be given. At time t_k a new measurement of the states in the form of (4.20) improves their estimation and the new covariance matrix at this epoch is given by

$$P_k = (I - K_k\,H)\,P_k^- \tag{4.25}$$

4.7 Kalman Smoothing

The smoothing problem with discrete measurements can be expressed as an estimate of the state vector at some time t_k based on a set of noisy measurements before *and after* this time. The INS system for the present application should interpolate positions between discrete GPS measurement updates. As such, the so-called fixed-interval smoothing is considered and assumed to be done post-mission. Fixed-interval smoothing yields an estimate $\delta\hat{x}_{k/N}$ for any time t_k within some interval: $k \in [0,1, ..., N]$. This type of smoothing can be done only in post-mission data

processing. The subscript notation "k/N" refers to the estimate of the state vector at time t_k on the basis of all measurements up to the end of the interval (i.e. up to t_N). For computational reasons, a recursive discrete smoothing algorithm is used, although other algorithms could be considered (e.g., batch least-squares).

The *mBF* (modified Bryson-Frazier) algorithm gives the smoothed estimate as a correction to the Kalman filter estimate for the same point. This method was proposed by Bierman (1973) for a continuous system with discrete measurement (see also Bierman, 1977). The smoothing is obtained by performing a Kalman-like recursion, backward in time, where the filtered states, $\delta\mathbf{x}_k$, and their covariances do not have to be saved, except at the point at which the smoothed estimate is desired. With appropriate definitions of a (so-called adjoint) variable, λ, and its covariance, Λ, the same algorithm used for the filter (forward sweep) can be used for the backward sweep. It is necessary, however, to save the following quantities computed in the filter cycle:

$$\boldsymbol{\varepsilon}_k = \delta\mathbf{y}_k - \mathbf{H}_k\,\delta\hat{\mathbf{x}}_k^- \quad \text{(predicted filter residual, or innovation)} \tag{4.26}$$

$$\mathbf{D}_k = \mathbf{H}_k\,\mathbf{P}_k^-\,\mathbf{H}_k^T + \mathbf{R}_k \quad \text{(predicted residual covariance)} \tag{4.27}$$

$$\mathbf{K}_k = \mathbf{P}_k^-\,\mathbf{H}_k^T\,\mathbf{D}_k^{-1} \quad \text{(Kalman gain)} \tag{4.28}$$

The equations associated with the backward filter are summarized in the following:

Initialization:

$$\boldsymbol{\lambda}_N^+ = 0 \tag{4.29}$$

$$\boldsymbol{\Lambda}_N^+ = 0 \tag{4.30}$$

where the superscript "+" denotes a time on the positive side of t_N, in this case, i.e. just ahead of the assimilation of the measurement at time t_N, if there is any.

Time propagation (note its backward character):

$$\boldsymbol{\lambda}_k^+ = \boldsymbol{\Phi}^T(t_{k+1},t_k)\,\boldsymbol{\lambda}_{k+1}^- \tag{4.31}$$

$$\boldsymbol{\Lambda}_k^+ = \boldsymbol{\Phi}^T(t_{k+1},t_k)\,\boldsymbol{\Lambda}_{k+1}^-\,\boldsymbol{\Phi}(t_{k+1},t_k) \tag{4.32}$$

Measurement update:

$$\boldsymbol{\lambda}_k^- = \boldsymbol{\lambda}_k^+ - \mathbf{H}_k^T\,\mathbf{D}_k^{-1}\,(\boldsymbol{\varepsilon}_k + \mathbf{D}_k\,\mathbf{K}_k^T\,\boldsymbol{\lambda}_k^+) \tag{4.33}$$

$$\Lambda_k^- = \left(I - K_k H_k\right)^T \Lambda_k^+ \left(I - K_k H_k\right) + H_k^T D_k^{-1} H_k \tag{4.34}$$

At those times when estimates of the smoothed state vector and its covariance are desired, they are computed from

$$\delta\hat{x}_{k/N} = \delta\hat{x}_k^{\pm} - P_k^{\pm} \lambda_k^{\pm} \tag{4.35}$$

$$P_{k/N} = P_k^{\pm} - P_k^{\pm} \Lambda_k^{\pm} P_k^{\pm} \tag{4.36}$$

Equations (4.35) and (4.36) work for either a priori and a posteriori quantities on the right side, as long as one is consistent. If no measurement updates exist within the interval (but they do exist at the endpoints of the interval), as is the case here, then only the time propagation equations (4.31) and (4.32) are implemented.

CHAPTER 5

TEST RESULTS

5.1 Introduction

The purpose of the tests conducted for this project was to demonstrate the feasibility of using INS to aid GPS in positioning an aircraft at a level of accuracy commensurate with that of GPS, with primary application in aerial photogrammetry where both GPS outages and the discreteness of the GPS positions may require such aiding. In addition, integration algorithms were to be developed and tested. The demonstration was to be conducted with actual data collected using a medium-to-high accuracy INS with a geodetic quality GPS receiver on board the ODOT photogrammetric aircraft.

The tests were planned around the availability of an LN93 INS, on loan from Litton through the Air Force Phillips Laboratory. In addition, the Center for Mapping at Ohio State University was constructing its own airborne GPS/INS platform using the Litton LN100 INS and Trimble 4100 GPS receivers. Data from their test flights would also be used to fulfill the requirements of this project.

A brief consideration of the aircraft in which the INS would be used brings to light some of the more mundane aspects of GPS/INS integration for a particular application. The airplane available to ODOT is a light, twin-engine, propeller aircraft, designated the Partenavia P68, built by Aeritalia. The GPS antenna is mounted on the fuselage above the camera that sits just aft of the second (and last) row of seat(s) in the aircraft. As thus configured, the weight budget for the aircraft is fairly tight and may allow for no more than an additional 50 kg (100 lbs). Aircraft power is 28 VDC (unregulated) and would be available for the INS up to several amperes. Finally, a desk-top/lap-top computer with appropriate interface to the must accompany the INS to control the system and collect the data. Generally, available INS's being designed mostly for military application use the RS 1553 data bus protocol. Special power considerations for the computer must also be made, including primarily that it is uninterruptable.

5.2 Tests with the LN93

The LN93 tests started with ground trials in the laboratory and in a van to establish the operational procedures and to confirm the advertised accuracy of the system. These tests were largely successful and were described in an intermediate progress report (Jekeli, 1997) and at the OTEC 1996 conference (Jekeli, 1996b). Figure 5.1 shows a local course driven three times with the INS and GPS (unfortunately GPS was not operating well due to user errors; also a power failure prevented one course from being completed). The misclosures of between 450 m and 900 m for the 0.75-hour trips verify that the LN93 is a system whose total error accumulates at the rate of about 1 km per hour. This is the advertised capability of the system and means that the individual components of the INS (three accelerometers and three gyros) are operating as specified.

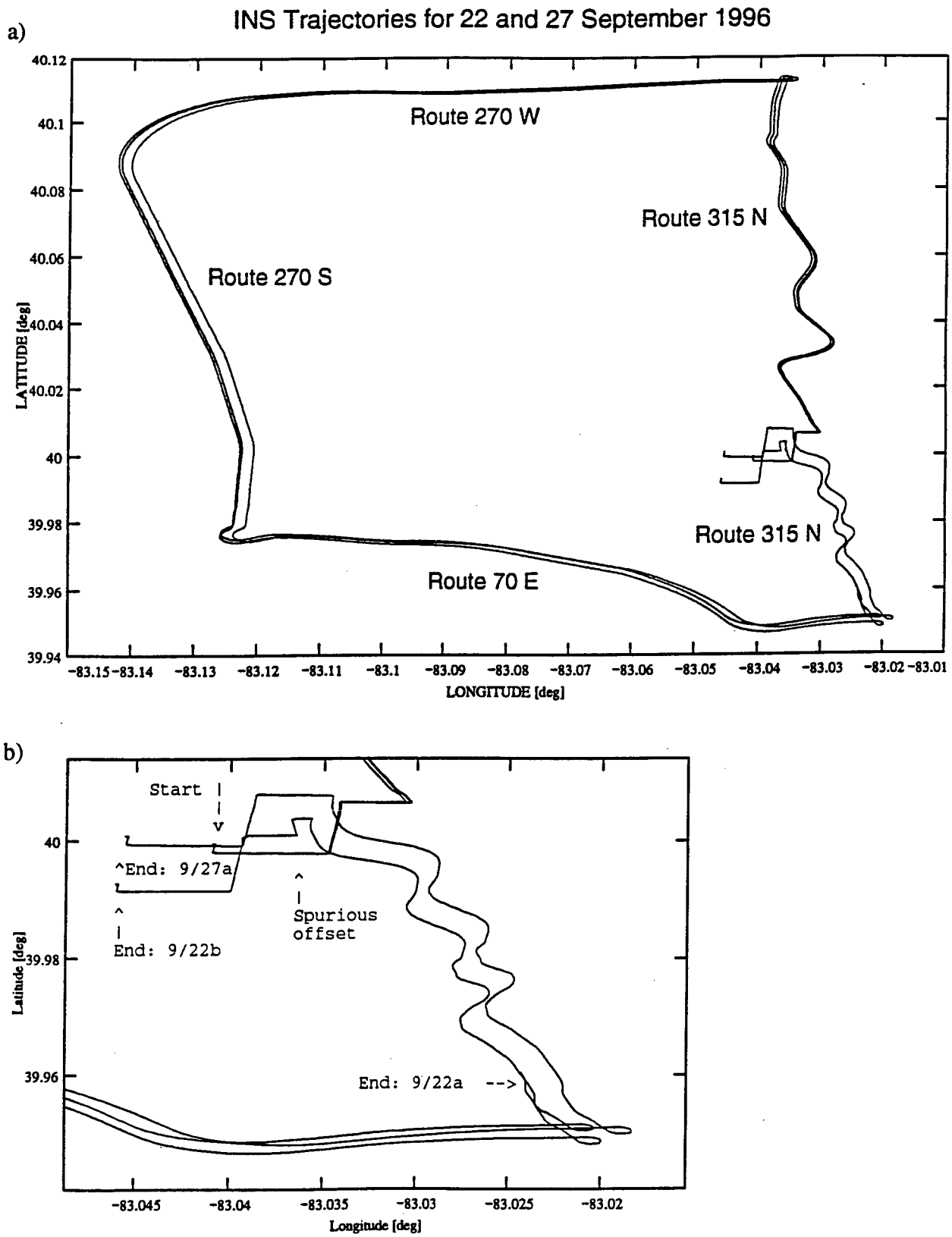

Figure 5.1: a) Local test course for the LN93 along highways in Columbus, OH.
b) Detail showing misclosures.

However, these and further preliminary achievements required much unplanned additional work for the following reasons. The INS interface software (the bus controller) required major modification to ensure proper synchronization of INS and GPS data. The synchronization is based on the timing signal (1 pps) from the GPS receiver. In addition, software changes were needed to allow interfacing to the Trimble GPS receiver (used by ODOT), rather than the Ashtech GPS receiver originally used by the Air Force. Other software changes include allowing manual height input to the INS when used on an aircraft where changes in altitude are significant (during ascent and descent; the INS does not navigate in the vertical). These software changes were hampered by the arcane coding (Pascal) of the Litton supplied "User Friendly Bus Controller" software.

A special uninterruptable power supply (UPS) was built at OSU for the laptop computer and a custom cage for the INS and laptop computer was built by ODOT for mounting in the Partenavia P68. These efforts were often delayed since they could only be done as time permitted. Several more serious delays occurred due to problems in the hardware of the computer and the interface boards, caused by faulty grounding and power failures that were difficult to isolate and correct. Other delays were caused by the unavailability of the GPS receiver (needed by ODOT's aircraft) for laboratory testing and the aircraft itself that could only be used if otherwise idle.

Although most these problems were resolved by the conclusion of the contract for this project, sufficient testing of the LN93 on the Partenavia was not possible. Only one test was conducted with the ODOT airplane, but unfortunately, a problem with the UPS, as well as a software error, prevented INS data from being collected by the laptop computer. Therefore, the numerical analyses that constitute the essential results for this project were conducted using test data obtained from the LN100 system and provided by the Center for Mapping.

5.3 Tests with the LN100

The LN100 is an inertial navigation system quite similar to the LN93, the only difference being in the type of gyros used. This newer generation of gyros allows considerable savings in power and weight for the system (see Table 3.1). The Center for Mapping conducted several test with the LN100 and a Trimble 4000 SSE receiver on board a twin engine, turbojet airplane by Beechcraft. One of these tests was a ten-minute flight in the St. Louis area, whose trajectory is shown in Figure 5.2. GPS data were collected on board the aircraft as well as at a ground station with data rate of 1 Hz. These data were processed by the Center for Mapping according to the algorithm described in Chapter 2, thus yielding latitude and longitude of the aircraft GPS antenna for every second of the total flight time. The estimated standard deviations of these positions are about 2-3 cm.

The raw accelerometer and gyro data from the LN100 were collected and processed by the Center for Mapping using their own navigation algorithm as outlined in Chapter 3 (rather than the one provided by Litton, as for the LN93). The result of this processing was the latitude and longitude of the aircraft as indicated by the INS at a data rate of 32 Hz.

To verify the position prediction and smoothing capabilities of the integration algorithms described in Chapter 4, the entire flight period was divided into 30-second intervals. On each alternate interval it was assumed that GPS positions are not available, representing outages due to loss of lock, or multiple successive cycle slips. The positions on those intervals were then computed on the basis of the INS data and compared to the positions actually available from GPS. Thus, the GPS positions serve as truth values during these intervals of presumed unavailability. It

was assumed that there is negligible rotation of the lever arm between the INS and GPS antenna, so that the relative positions determined by the INS are reasonably accurate extrapolations / interpolations of the GPS antenna position.

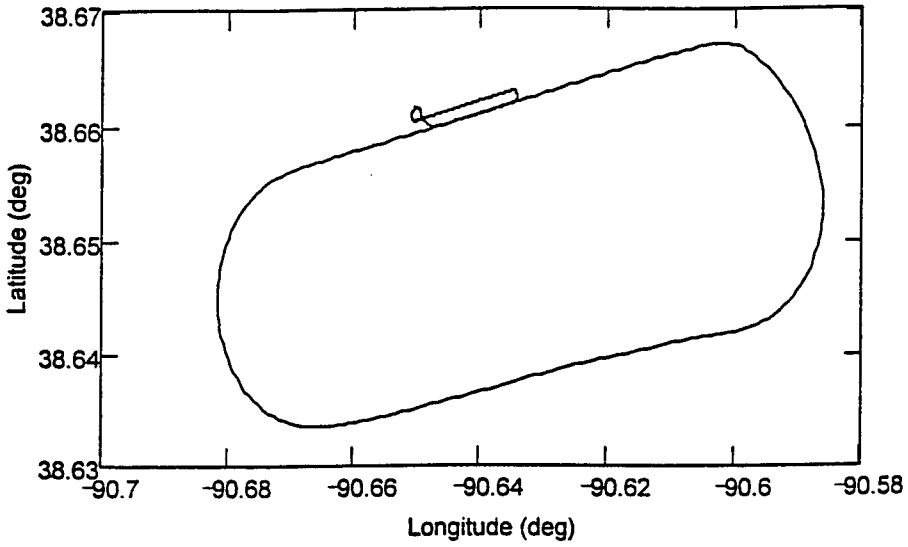

Figure 5.2: AIMS test flight #2, Center for Mapping, OSU.

Figure 5.3 shows the difference between INS and GPS positions (latitude and longitude) when INS is allowed to navigate in the free-inertial mode for the entire flight, where at the beginning of each GPS outage the INS positions are reset to the (last known) GPS positions. This corresponds to the uncoupled integration shown schematically in Figure 4.1. Figure 5.4 shows the difference between INS and GPS positions during the "outages" in the case that INS errors are estimated (calibrated) while GPS positions are available. The INS positions are determined on the basis of the error propagation equation (4.21), where the INS sensor errors were estimated using the Kalman filter algorithm described by equation (4.22) when GPS position observations were available. This corresponds to the loose integration depicted schematically in Figure 4.2. Finally, Figure 5.5 shows the differences between INS and GPS positions in the case that the INS position errors are estimated using Kalman smoothing, as outlined in Section 4.7. This is similar to the previous case of loose integration, but makes further use of the fact that GPS outages are finite in duration (in this example, they last 30 seconds). Table 5.1 compares these three types of integration in terms of some essential statistics: absolute maximum and root-mean-squares of middle and endpoint differences in INS and GPS position coordinates over all outage intervals.

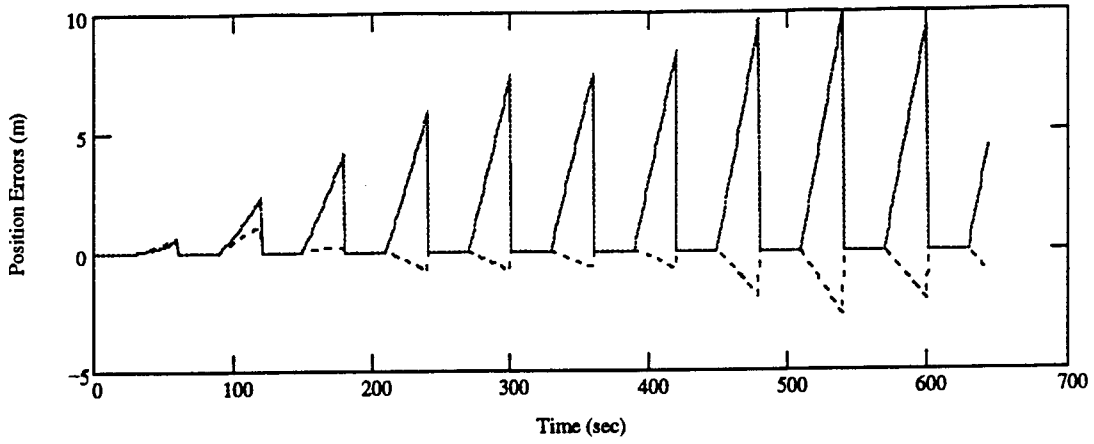

Figure 5.3: Differences between GPS and INS determined coordinates in latitude (solid line) and longitude (dotted line) during presumed GPS outages, for the case of uncalibrated INS errors.

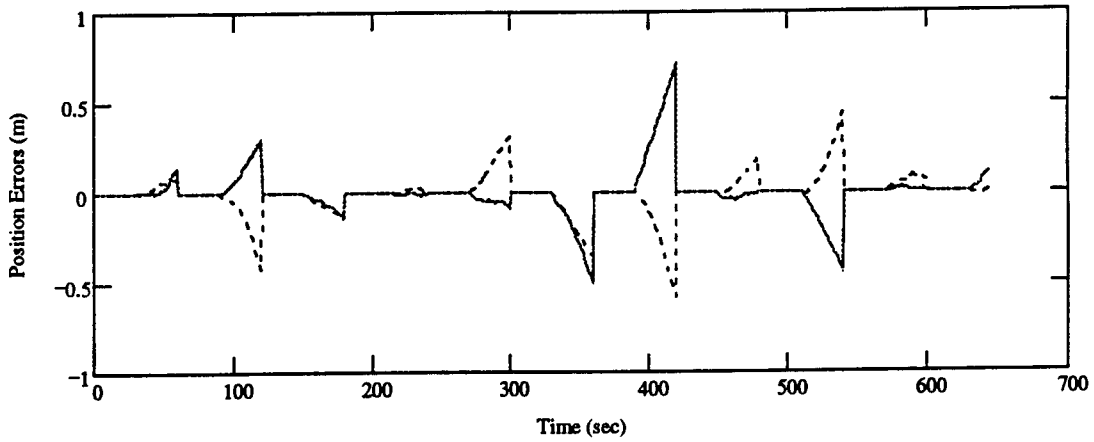

Figure 5.4: Differences between GPS and INS determined coordinates in latitude (solid line) and longitude (dotted line) during presumed GPS outages, for the case of calibrated INS errors using the Kalman filter.

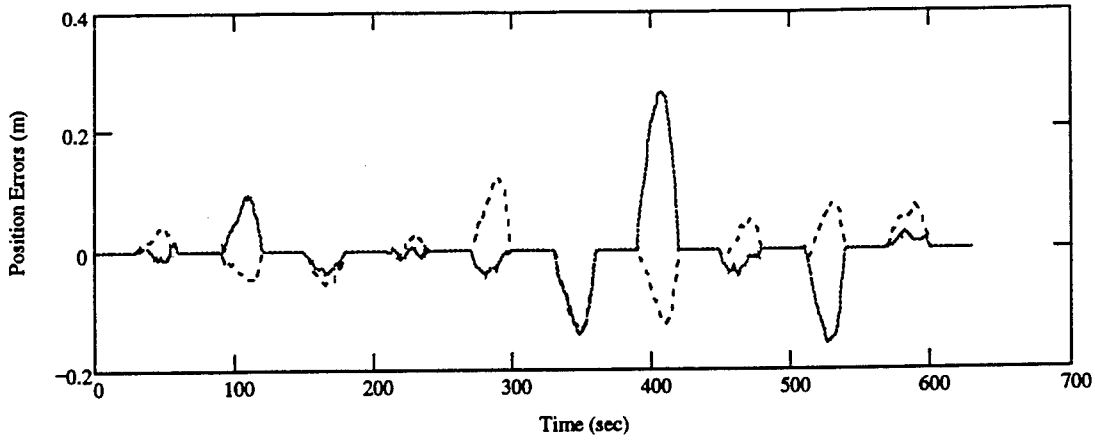

Figure 5.5: Differences between GPS and INS determined coordinates in latitude (solid line) and longitude (dotted line) during presumed GPS outages, for the case of calibrated INS errors using the Kalman filter and smoother.

Table 5.1: Summary of differences between INS and GPS coordinates based on unfiltered, filtered, and filtered and smoothed INS errors. All values are in [meters].

	Max. Abs. Diff. [m]		RMS Difference middle of outage [m]		RMS Difference end of outage [m]	
	lat.	lon.	lat.	long.	lat.	lon.
Uncalibrated INS	9.92	2.72	3.775	0.746	7.15	1.40
Kalman filtered INS	0.682	0.589	0.153	0.115	0.326	0.314
Filtered & smoothed INS	0.260	0.123	0.106	0.070	0	0

CHAPTER 6

SUMMARY

The objectives of this project have been achieved and the results of the work are described in this report. Chapter 1 discusses the motivation and objectives of the project. Chapters 2 and 3 detail and compare the GPS and INS positioning systems to be considered. The algorithms for integrating the two systems for practical implementation are reviewed in Chapter 4. And, the results of test data analyses are presented in Chapter 5. While considerable knowledge has been gained in configuring an integrated GPS/INS platform using the LN93, this latter system failed to become operational for test purposes during the period of this contract. The test data results described in Section 5.3 and below refer to the LN100 INS that was operated by the Center for Mapping. This INS is practically equivalent in terms of accuracy, but more versatile in terms of operation and implementation.

From Figures 5.3, 5.4, and 5.5 it is evident that INS positioning is a valuable aid to GPS positioning when the latter is unavailable for short periods of time. A comparison of Figure 5.3 with Figures 5.4 and 5.5 further shows that the integration of INS and GPS requires some form of optimal estimation algorithm to achieve decimeter level accuracies during prolonged (30 second) outages of GPS. The differences shown in the figures and synopsized in Table 5.1 do not account for errors in GPS and thus are not total errors in INS-derived positions. However, since the GPS-estimated positions have standard deviations on the order of 2-3 cm, these differences are close to the total position errors. In summary, integration of GPS with an INS of the quality of the LN100 will support continuous aircraft positioning accuracy at the 10 cm level for GPS outages up to 30 seconds, and better for shorter outages. This is also entirely adequate to recover from cycle slips over that interval, since it represents only half of one wavelength of the carrier wave.

It is noted that these results are much more pessimistic than predictions made under a previous ODOT feasibility study (Jekeli, 1995). These predictions were based on longer calibration periods for INS sensor errors than allowed here. This means that the quality of the INS recommended in (Jekeli 1995), being of the LN100 type, is even more justified by the results of this report. Recent studies by Wang and Jekeli (1998) show that improved modeling of position errors can reduce the INS-derived positions from a calibrated, smoothed solution, such as above, to the level of the GPS positional accuracy of 2-3 cm.

Finally it is noted that angular data from the gyros of the INS is a by-product that could be used to provide orientation information to the photogrammetric camera. The algorithms developed here yield improved estimates of gyro drift and could be implemented to provide accurate orientation of the camera at the times of exposure. In addition, the algorithm can be augmented with better models that include correlated gyro errors.

To implement the GPS/INS integration studied under this project in an actual operational setting requires a dedicated GPS/INS system and software development. Most of the groundwork for such a system has been laid with this and previous studies in terms of feasibility, hardware configuration and integration, accuracy demonstration, and algorithmic development. The next step would be the procurement of an LN100 INS, GPS receiver, and ancillary computer equipment for the development of an integrated GPS/INS platform on ODOT's Partenavia P68.

Acknowledgments: The preparation of this report and associated numerical analyses were supported by Ohio Department of Transportation, Research Project: "Continuous Aircraft Positioning Using GPS Aided by INS," State Job No. 14643(0). Many individuals contributed to the success of this project. Among the graduate students at OSU who had a significant input are Bishnu Phuyal, Patrick Gakure, and Fathi Dwaik; Dr. Jin Wang, post-doctoral researcher at OSU, adapted his software to conduct some of the numerical tests; the Center for Mapping (Dr. John Bossler and his staff) kindly provided the processed GPS and INS data; Frank Huffman, Design Engineer, built the uninterruptable power supply; Air Force Phillips Laboratory loaned the LN93 to OSU and supported Dr. Ian Humphrey, Fibersense Corp., to help in the GPS / INS time synchronization; Paul Redman, Aircraft Maintenance Superintendent, ODOT Aviation Division, supervised the construction of the INS platform for aircraft testing and was very helpful in arranging the flight test.

REFERENCES

Bierman, G.J., 1973: "Fixed interval smoothing with discrete measurements." *Int. J. Control*, **18**(1), 65-75.

Bierman, G.J., 1977: *Factorization Methods for Discrete Sequential Estimation.* Academic Press, New York.

Britting, K.R., 1971: *Inertial Navigation Systems Analysis*, Wiley Interscience, Wiley & Sons, New York.

Brokowski, K.M., 1989: "Accurate algorithms to transform geocentric to geodetic coordinates." *Bulletin Géodésique*, 63, 50-56.

Brown, R.G., 1983: *Introduction to Random Signal Analysis and Kalman Filtering.* Wiley & Sons, New York.

Gelb, A., 1974: *Applied Optimal Estimation*, M.I.T. Press., Massachusetts.

Jekeli, C., 1994: "Airborne vector gravimetry using precise, position-aided inertial measurement units." *Bulletin Géodésique*, 69, 1-11.

Jekeli, C., 1995: "A review of using an inertial navigation system to aid GPS in accurate positioning of an aerial photogrammetric platform." In Final report for ODOT, State Job No. 14565(0)., Report No. FHWA/OH-96/001, December, 1995.

Jekeli, C., 1996a: "Inertial Geodesy." Lecture Notes prepared for OSU course GS694, Spring Quarter, 1996.

Jekeli, C., 1996b: "Accurate Kinematic Positioning Using Global Positioning System and Inertial Navigation System." Presented at 1996 OTEC Conference, Columbus, OH, 19-20 November, 1996.

Jekeli, C., 1997: "Progress Report on Continuous Aircraft Positioning Using GPS Aided by INS for Quarter Ending 12/31/96." ODOT, State Job No. 14643(0)., February, 1997.

Leick, A., 1995: *GPS Satellite Surveying*, John Wiley and Sons, Inc., New York.

Moritz, H., 1980: *Advanced Physical Geodesy*, Abacus press, Tunbridge Wells, Kent.

Schwarz, K.P., N. El-Sheimy, and Z. Liu, 1994: "Fixing GPS cycle slips by INS/GPS - methods and experiences." Proc. Internat. Symp. Kinematic Systems in Geodesy, Geomatics, and Navigation, 30 August - 2 September 1994, Banff, Canada, pp.265-275.

Söhne, W. and O. Heinze, 1995: "Precise positioning with INS and GPS in land vehicle and flight application." Proceedings of the Third International Workshop on High Precision Navigation, K. Linkwitz and U. Hangleiter (eds.), pp.311-317, April 1995, University of Stuttgart, Dümmler Verlag, Bonn.

Yang, M., 1995: New GPS measurement modelling techniques of orbit determination and precise kinematic positioning. Report No.431, Department of Geodetic Science and Surveying, Ohio State University, Columbus, Ohio.

Wang, J. and C. Jekeli, 1998: "Statistic model versus deterministic model in INS/GPS positioning." paper to be submitted to Journal of Geodesy.